Ocean Engineering 35 (2008) 1388–1400

Contents lists available at ScienceDirect

Ocean Engineering

journal homepage: www.elsevier.com/locate/oceaneng

Wave interaction with low-mound breakwaters using a RANS model

J.L. Lara *, I.J. Losada, R. Guanche

Environmental Hydraulics Institute (IHCantabria), Universidad de Cantabria, Avda. de los Castros s/n. 39005 Santander, Spain

ARTICLE INFO

Article history:
Received 25 October 2007
Accepted 21 May 2008
Available online 1 June 2008

Keywords:
Breakwaters
Wave overtopping
Numerical analysis
Coastal structures

ABSTRACT

Using COBRAS-UC, a numerical model based on the Volume-Averaged Reynolds Average Navier–Stokes (VARANS) equations, 2-D wave interaction with low-mound breakwaters is analyzed. The model uses a Volume of Fluid (VOF) technique method to capture the free surface which allows the modeling of complicated processes such as breakwater overtopping. Furthermore, thanks to the VARANS equations, the flow in the permeable layers underneath the caisson is quantitatively correct. In order to validate the model's performance, a new set of experimental studies are carried out in a wave flume at a 1:20 scale using regular and irregular waves. Comparisons between numerical and experimental free surface, pressure time histories, and overtopping layer thickness for regular and irregular waves show a good agreement. Further comparisons of numerically predicted overtopping magnitudes with existing semi-empirical formulae and experimental data indicate that the model can be used as a complementary tool for the functional design of this kind of structures.

1. Introduction

Coastal structures are built to protect coastal areas from erosion and flooding, as well as to shelter ports and marinas from wave action. The wave and structure interaction process depends on incident wave conditions and the structure typology.

In order to provide design guidelines for the hydraulic response of coastal structures, many semi-empirical formulations based on flume and basin experiments have been developed in the past. Such formulae try to consider and parameterize the most relevant variables ruling the process which occurs in the wave and structure interaction phenomenon, mainly, reflection, run-up, rundown, overtopping and transmission. An extensive number of very successful semi-empirical formulations are available in the literature and can be found, as part of the state of the art in coastal structure designs, in several books and manuals (e.g. Burcharth and Hughes, 2006).

As previously stated, semi-empirical formulations, based on flume or wave basin experiments, cover a limited number of typologies and setups. Furthermore, many of them are based on a reduced set of incident wave conditions, which may lead to uncertainties and errors if used out of range, a problem often faced in current design or pre-design conditions.

In recent years, computational modeling of wave interaction with coastal structures is becoming an important complementary approach, especially when pre-designing the hydraulic response of some typologies of coastal structures.

The numerical model ability to successfully analyze wave and structure interaction problems depends mainly on the equations and solving techniques used, Losada (2003). Moreover, the leap to its application on real case studies requires computational robustness and efficiency in terms of computation as well as a thorough validation process which is only available today for a limited set of models.

According to the existing literature, the most relevant numerical models currently available for wave and coastal structures interaction are different versions of models solving the nonlinear shallow equations; models based on Reynolds Average Navier–Stokes equations (RANS) including any kind of free surface-tracking or capturing technique and, more recently, particle methods such as the Smoothed Particle Hydrodynamics (SPH). In this last model the governing partial differential equations of continuum fluid dynamics, are transformed into particle form by integral equations through the use of an interpolation function that gives kernel estimation of the field variables at a point.

Models based on nonlinear shallow water equations (NSWE), are derived on the assumption of hydrostatic pressure and are obtained by vertically integrating the Navier–Stokes equations (NSE), i.e. Kobayashi and Wurjanto (1989), Mingham and Causon (1998), Hu et al. (2000), Hubbard and Dodd (2002) and Stansby and Feng (2004). The use of NSWE places severe restrictions on real applications inherent, essentially, to the intrinsic requirement to satisfy the shallow water limit. This restriction is especially harsh when considering high frequency components in the

* Corresponding author. Tel./fax: +34 942 20 18 10.
E-mail address: lopezjav@unican.es (J.L. Lara).

0029-8018/$ - see front matter © 2008 Elsevier Ltd. All rights reserved.
doi:10.1016/j.oceaneng.2008.05.006

incident wave spectrum and also requires locating the offshore boundary condition of the numerical model close to the structure. Other restrictions are associated with the semi-empirical introduction of breaking, porous flow modeling or the difficulty in simulating complicated free surfaces. However, they are computationally very efficient in providing the possibility to simulate wave trains including about 1000 waves very rapidly, which may be of importance, for example, when analyzing extreme statistics of wave overtopping.

The inherent limitation of the shallow water limit may be overcome considering the application of modified Boussinesq equations for wave and structure interactions (e.g. Lynett et al., 2000). However, the computational effort required to solve these equations has discouraged researchers in using them for real applications.

During the last years particle methods such as the Moving Particle Semi-Implicit (MPS) method of Koshizuka et al. (1995); or the SPH method in its different versions (i.e. Dalrymple et al., 2001; Gotoh et al., 2004; Shao, 2006) have become very popular. Being based on a grid-less Lagrangian approach, they are able to accurately track large deformations of the free surface. However, whether or not the weakly incompressible or the incompressible SPH method is used, this technique has several disadvantages. The high number of particles required to obtain a reliable solution; the use of fixed particle spacing; the limited validation available and a very low computational efficiency are some of the issues that need to be solved before considering SPH for practical purposes.

Free of some of the mentioned limitations above, numerical models based on the NSE have received considerable attention in the last decade applied to the analysis of wave interaction with coastal structures under breaking conditions, as they allow the calculation of the velocity field in the whole computational domain for any type of flow, whether rotational or irrotational.

Among existing NSE models, RANS-based equation models are nowadays the more suitable tool to analyze the wave–structure interaction problem. The analysis of wave interaction with porous structures lies in the fact that they take into account the turbulence generation/dissipation mechanisms inside the porous media and also in the wave breaking process. The introduction of the turbulent effects constitutes a true stumbling block for the modeling of wave–structure interaction with permeable breakwaters. Among other RANS models available in literature (i.e. Troch and de Rouck, 1998; Kawasaki, 1999; Li et al., 2004), COBRAS is probably the most extensively validated, especially for wave–structure interaction.

Lin and Liu (1998), based on a previously existing model called RIPPLE (Kothe et al., 1991), presented COBRAS (Cornell Breaking Waves and Structures) for simulating breaking waves and wave interaction with coastal structures. In this work, a modified and improved version of COBRAS, named COBRAS-UC (Losada et al., 2008; Torres-Freyermuth et al., 2007) is used to investigate the interaction of regular and irregular waves with low-mound breakwaters focusing on the hydraulic response of the structure. According to the PROVERBS parameter map, Oumeraci et al. (2001), low-mound breakwaters are characterized by a relative height $0.3<h_b^*=(h_b/h)<0.6$, where h_b is the mound foundation height and h is the water depth in front of the structure. Depending on the relative wave height, this structure typology might be subjected to quasi-standing wave loads or impact wave loads. Please note, that the quasi-standing wave load response is not usually expected for composite breakwaters. In terms of hydraulic response low-mound breakwaters are closer to vertical breakwaters than rubble-mound breakwaters and therefore reflection dominates the structure response and potential overtopping. Wave breaking is not relevant in this case and the porous flow is limited. Therefore, the modeling presented in this paper is very different to the case considered in Losada et al. (2008) in which the hydraulic response, run-up and overtopping are dominated by the wave breaking process on the breakwater rubble-mound layers.

The paper is organized as follows. The main characteristics of COBRAS-UC are presented in the following section. The experimental setup carried out for the model validation is presented followed by an explanation of the numerical setup and model calibration. The next section is devoted to the numerical model validation through the comparison of the numerical and experimental results of free surface and pressure time series, wave spectra and several overtopping related magnitudes. A specific section on the application of the model to wave overtopping analysis can be found next. The paper is completed with some comparisons between results of low-mound and rubble-mound breakwaters, recommendations for numerical modeling based on the experience achieved and conclusions.

2. Mathematical formulation

2.1. Equations in the fluid domain

COBRAS-UC (Losada et al., 2008) solves the 2DV RANS equations, based on the decomposition of the instantaneous velocity, u, and pressure field, p, into mean, $\overline{\cdot}$, and turbulent components, $'$:

$$\frac{\partial \overline{u_i}}{\partial x_i}=0, \tag{1}$$

$$\frac{\partial \overline{u_i}}{\partial t}+\overline{u_j}\frac{\partial \overline{u_i}}{\partial x_j}=-\frac{1}{\rho}\frac{\partial \bar{p}}{\partial x_i}+g_i+\frac{1}{\rho}\frac{\partial \overline{\tau_{ij}}}{\partial x_j}-\frac{\partial(\overline{u_i'u_j'})}{\partial x_j}, \tag{2}$$

and the k–ε equations for the turbulent kinetic energy (k), and the turbulent dissipation rate (ε):

$$\frac{\partial k}{\partial t}+\overline{u_j}\frac{\partial k}{\partial x_j}=\frac{\partial}{\partial x_j}\left[\left(\frac{\upsilon_t}{\sigma_k}+\upsilon\right)\frac{\partial k}{\partial x_j}\right]-(\overline{u_i'u_j'})\frac{\partial \overline{u_i}}{\partial x_j}-\varepsilon, \tag{3}$$

$$\frac{\partial \varepsilon}{\partial t}+\overline{u_j}\frac{\partial \varepsilon}{\partial x_j}=\frac{\partial}{\partial x_j}\left[\left(\frac{\upsilon_t}{\sigma_\varepsilon}+\upsilon\right)\frac{\partial \varepsilon}{\partial x_j}\right]+C_{1\varepsilon}\frac{\varepsilon}{k}\upsilon_t\left(\frac{\partial \overline{u_i}}{\partial x_j}+\frac{\partial \overline{u_j}}{\partial x_i}\right)\frac{\partial \overline{u_j}}{\partial x_i}-C_{2\varepsilon}\frac{\varepsilon^2}{k}, \tag{4}$$

where $i, j=1, 2$ for a two-dimensional flow, ρ is the density of fluid, g_i is the ith component of the gravitational acceleration, $\overline{\tau_{ij}}$ is the viscous stress tensor of the mean flow and υ_t is the eddy viscosity. For a Newtonian fluid, $\overline{\tau_{ij}}=2\mu\overline{\sigma_{ij}}$, with μ being the molecular viscosity and $\overline{\sigma_{ij}}=1/2(\partial\overline{u_i}/\partial x_j+\partial\overline{u_j}/\partial x_i)$, the rate of strain tensor of the mean flow.

The influence of turbulence fluctuations on the mean flow field is represented by the Reynolds stresses $\rho(\overline{u_i'u_j'})$. The governing equations for k–ε are derived from the NSE, and higher order correlations of turbulence fluctuations in k and ε equations are replaced by closure conditions. The empirical coefficients ($C_{1\varepsilon}=1.44$; $C_{1\varepsilon}=1.92$; $\sigma_\varepsilon=1.3$ and $\sigma_k=1.0$) were experimentally determined from stationary flows, Rodi (1980). A nonlinear algebraic Reynolds stress model is used to relate the Reynolds stress tensor and the strain rate of mean flow (see Rodi, 1980; Lin and Liu, 1998, for details). The movement of free surface is tracked by the Volume of Fluid (VOF) method.

2.2. Equations for the flow in the porous media

The main assumption of the COBRAS-UC model is to consider that the RANS equations coupled with an appropriate turbulence

model (in the present case, the k–ε model) can adequately describe the flow field in the porous media. Given the complex structure of porous materials, the direct resolution of the intrinsic flow field inside the pores is still not practical.

Consequently, the flow in porous media is obtained in the COBRAS-UC model through the resolution of the Volume-Averaged Reynolds Averaged Navier–Stokes (VARANS) equations; see Hsu et al. (2002) for the complete mathematical formulation. These equations are derived by integrating the RANS equations over a control volume. The mathematical process of volume averaging of a certain quantity a is defined by the following expression:

$$\langle a\rangle = \frac{1}{V_f}\int_{V_f} a\,dV, \tag{5}$$

where $\langle\ \rangle$ denotes the intrinsic volume averaging, V is the total averaging volume, V_f is the volume in V which is occupied by the fluid phase and $\langle a\rangle$ is the averaged magnitude. The intrinsic averaging operator defined by Eq. (5) can be related to Darcy's volume averaging operator defined as follows:

$$\langle K\rangle_D = \frac{1}{V}\int_{V_f} a\,dV, \tag{6}$$

through the simple relationship: $\langle a\rangle_D = n\langle a\rangle$, where $n = V_f/V$, is the porosity and for simplicity it is assumed to be a constant in the present model. In terms of velocity, $\langle a\rangle_D$ would be the seepage velocity and $\langle a\rangle$ the filtration velocity. Hereafter, unless specified, volume averaging will be understood as intrinsic volume averaging, as defined in expression (5).

The VARANS equations are obtained by applying the intrinsic volume average to the RANS equations. The ensemble averaged velocity of the RANS equations (mass and momentum) are assumed to be:

$$\frac{\partial\langle\overline{u_i}\rangle}{\partial x_i} = 0, \tag{7}$$

$$\frac{\partial\langle\overline{u_i}\rangle}{\partial t} + \frac{\langle\overline{u_j}\rangle}{1+c_A}\frac{\partial\langle\overline{u_i}\rangle}{\partial x_j} = \frac{1}{\rho(1+c_A)}\left[-\frac{\partial\langle\overline{p}\rangle}{\partial x_i} - \frac{\partial\rho\langle u_i' u_j'\rangle}{\partial x_j} + \frac{\partial\langle\overline{\tau_{ij}}\rangle}{\partial x_j} + \rho g_i\right] - \frac{1}{1+c_A}\left[\frac{\alpha\nu(1-n)^2}{n^2 D_{50}^2}\langle\overline{u_i}\rangle + \frac{\beta(1-n)}{nD_{50}^2}\sqrt{\langle\overline{u_1}\rangle^2 + \langle\overline{u_2}\rangle^2}\langle\overline{u_i}\rangle\right]. \tag{8}$$

In the VARANS equations, the interfacial forces between the fluid and solids have been modeled according to the extended Forchheimer relationship, in which both linear and nonlinear drag forces are included in the last term of Eq. (8).

The expression used in the model for the linear and nonlinear drag forces is given by:

$$I = \frac{\alpha\nu(1-n)^2}{n^2 D_{50}^2}\vec{u} + \frac{\beta(1-n)}{n^2 D_{50}}\vec{u}|\vec{u}|, \tag{9}$$

where α and β are the only two empirical parameters used in the calibration of the numerical model, n is the porosity, ν is the kinematic viscosity and $\vec{u}$ stands for velocity. An additional parameter, c_A, affecting the inertia term is included in the formulation to take into account the added mass. The precise descriptions of the α and β coefficients are still not fully understood for oscillatory flows. They depend on several parameters such as the Reynolds number, the shape of the stones, the grade of the porous material, the permeability, and of course, the flow characteristics. Based on previous work, we have experienced (Garcia et al., 2004; Lara et al., 2006a, b) that, under oscillatory flow and waves propagating over slopes or breaking, values existing in the literature may not be valid since the experimental conditions for obtaining those formulae did not take these effects into account. Detailed discussions on the numerical algorithms, initial and boundary conditions can be found in Lin and Liu (1998) and Hsu et al. (2002).

Over the last years, the model has been under a continuous development process based on an extensive validation procedure, carried out for low-crested structures (Garcia et al., 2004; Losada et al., 2005; Lara et al., 2006a), wave breaking on permeable slopes (Lara et al., 2006b), surf zone hydrodynamics on natural beaches (Torres-Freyermuth et al., 2007) and overtopping on rubble-mound breakwaters (Losada et al., 2008). In this last paper COBRAS-UC, a new version including a number of modifications introduced into the original COBRAS code at the University of Cantabria in order to overcome some of the initial limitations is presented. Thanks to the implemented modifications, the computational cost of the model has been reduced by 40% compared to the initial code for a typical run, and several sources of error which led to execution problems have been eliminated; allowing the consideration of larger and more complex computational domains, and longer simulation times.

In order to extend COBRAS-UC range of application, in this paper, further validation of the model is carried out by considering random wave interaction with low-mound breakwaters, a structure typology with a hydraulic and wave load response different from rubble-mound breakwaters.

Free surface, pressure and wave overtopping related parameters are analyzed based on the numerical model and compared with experimental results.

3. Description of the experimental setup

A set of experiments on wave interaction with a low-mound breakwater were carried out in the wave flume of the University of Cantabria. The flume is 60.5 m long, 2 m wide and 2 m high. At one side of the wave flume the mixed piston-pendulum type wave maker has two free surface wave gauges integrated in an Active Wave Absorption System (AWACS®) allowing the absorption of reflected waves. At the rear end of the wave flume, three dissipative ramps were placed to absorb the transmitted waves.

The breakwater (see Fig. 1) is built out of an impermeable caisson installed on a rubble-mound foundation. The impermeable caisson is 1.04 m long, 0.3 m high and 2 m wide. The still water level was 0.8 m, and the structure freeboard was 0.2 m. A 0.3 m high, $D_{50} = 0.035$ cm and 1V/2H gravel foundation was placed below the breakwater. The foundation layer was covered with an external layer of gravel with $D_{50} = 3.5$ cm. At the seaside face of the structure, a 10 cm berm was built. The porosity was 0.48 for the foundation layer and 0.50 for the outer layers.

Free surface evolution was measured using resistive gauges (WG) located along the flume. These were placed along the centreline of the wave flume in order to measure free surface time series. Ten wave gauges were located in front of the structure, three were used to evaluate the reflection coefficient. Three additional wave gauges were placed on the top of the caisson to measure the thickness of the water layer during the overtopping events. One wave gauge was placed at the leeward side of the structure to control water level in the flume. Finally, a reservoir was built at the crown of the structure in order to collect the water overtopping the structure. The top of the reservoir was aligned with the upper face of the caisson so as not to interfere with the flow. The box only occupied a third of the width of the wave flume, allowing most of the overtopped flow to reach the leeward side of the structure. A resistive wave gauge placed inside the pool recorded the free surface variation. The overtopping

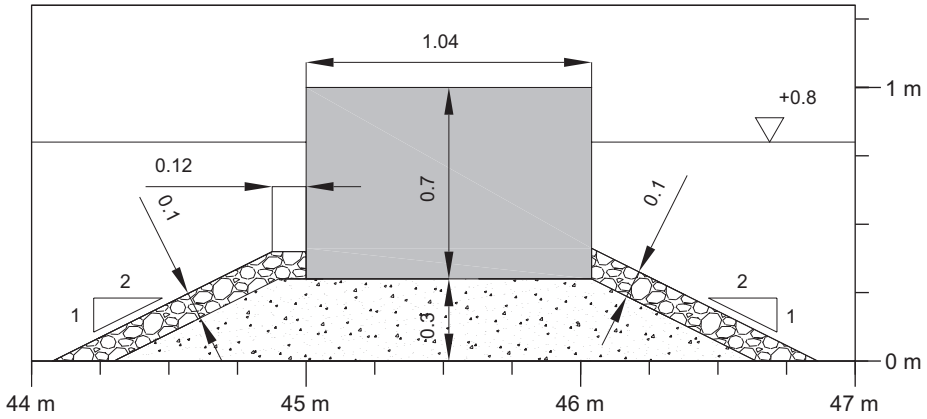

Fig. 1. Experimental setup. Data in meters.

Table 1
Target parameters for generated waves

Wave type		Regular		Irregular
Wave height	H (m)	0.1, 0.15, 0.2, 0.225,0.25	H_s (m)	0.084, 0.12, 0.15, 0.18, 0.21
Wave period	T (s)	2, 3, 4, 5, 6	T_p (s)	2, 3, 4, 5, 6
Water depth at wave paddle	h (m)	0.8	h (m)	0.8
Water length at wave paddle	L (m)	4.89–16.56	L (m)	4.89–16.56
Wave steepness	H/L	0.00604–0.0511	H_s/L	0.005724–0.0429
Relative freeboard	F/H	0.8–2	F/H_s	0.95–2.38
Relative crest width	B/L	0.0604–0.204	B/L	0.0604–0.204
Relative wave height	H/h	0.125–0.3125	H_s/h	0.104–0.2625
Relative depth	h/L	0.0483–0.1636	h/L	0.0483–0.1636

discharge was evaluated by measuring the water volume jumps in the reservoir of each overtopping wave. The water depth multiplied by the horizontal area of the reservoir (0.69 m^2) gives the instantaneous volume of water inside the box.

Six pressure transducers (PG) were installed at the front wall and four underneath the caisson to measure pressure time series, sampled at 60 Hz. Fig. 1 presents the experimental setup.

Regular and irregular waves were considered in the experiments. Fifth-order Stokes waves were generated for the regular wave cases. A JONSWAP-type spectrum ($\gamma = 3.3$) was considered for the random wave tests. The total number of different wave conditions was 20 for regular and 25 for random waves. Table 1 presents target wave conditions in the experimental setup.

A preliminary analysis of the experimental results clearly shows that the low-mound breakwater wave interaction is significantly dominated by wave reflection. Evaluated wave reflection reaches maximum values up to 95% and a minimum of 85% for cases including large overtopping volumes. An important additional observation is that the low-mound is not relevant enough to generate wave breaking and for most incident wave conditions the wave load response corresponds to a quasi-standing wave case. In Losada et al. (2008), the response of the rubble-mound breakwater is characterized by reflection with values ranging from 40% to 65%, and wave breaking on the breakwater slope. The correct modeling of the run-up on the permeable layers is the limiting factor for an accurate modeling of wave overtopping.

4. Numerical model setup and calibration

Following the experimental setup and previous experience in the application of the numerical model, incident waves are generated by an internal wave generator able to generate regular and irregular waves (Lara et al., 2006a).

The choice of grid size varies in the y-direction from 1 cm above the SWL (region 1) to 3 cm under the SWL (region 2). In the x-direction a coarser grid size, 5 cm, is used in the generation region, increasing the resolution up to 2 cm in the vicinity of the breakwater, which is the area of interest (region 3). A total number of 92 grids are used in the y-direction, while in the x-direction 2325 grids are used. Other grid resolutions have been tested in order to evaluate the computational time and the accuracy of the results. Using a resolution of 0.5 cm in both the horizontal and vertical direction increases computational time to a factor of 30 without much improvement in the accuracy of the results but with a better definition of the tongue of water overtopping the structure.

A sponge layer has been placed in region 1 in order to absorb the energy reflected on the structure and the waves generated by the internal source function in the offshore direction, requiring a numerical domain 25 m longer than the laboratory wave flume. In this case, absorption of re-reflected waves is extremely relevant due to the high reflection induced by the low-mound breakwater.

The only calibration parameters used in this model are the α (linear drag parameter) and β (nonlinear drag parameter) coefficients of the porous flow model (see Garcia et al., 2004; Lara et al., 2006a, b; Losada et al., 2008), as the remaining coefficient regarding the added mass, c_A is set to be 0.34 based on previous experience. In this work the best-fit values for α and β are evaluated by comparing experimental data and numerical results of free surface and pressure time series for two regular wave cases: (1) $H = 0.1$ m and $T = 3$ s and (2) $H = 0.1$ m and $T = 5$ s.

After a trial and error process, the best-fit parameter values calculated were $\alpha = 200$ and $\beta = 0.8$ for the foundation core and

$\alpha = 200$ and $\beta = 1.1$ for the external layer. Numerical results appeared to be more sensitive to the nonlinear drag coefficient β than to the linear drag parameter α, because the flow is mainly turbulent within the porous media. These values of the coefficients remain unchanged for all the other regular and irregular simulated wave cases. Please note that the model has been calibrated for only two of the total number of simulated tests.

5. Model validation

Model validation is carried out by comparing the numerical results with experimental measurements, as well as with semi-empirical formulations for some of the functional parameters for regular and irregular waves. In order to show the quality of the validation, selected results are presented.

5.1. Free surface time series

Results of free surface time series are presented in Fig. 2 for $H_s = 0.18$ m and $T_p = 5$ s; where H_s and T_p are the significant wave height and peak period, respectively.

Results are presented for eight positions; five in front of the structure and three over the crown. Plotted results include a simulation time of 160 s with approximately 50 waves in the time series. The agreement between the numerical results and the measurements for both wave phase and height is very good. The model is able to simulate the quasi-standing wave pattern with a quasi-antinode located at the caisson and the quasi-node close to WG7. Waves increase their steepness due to reflection and shoaling on the permeable layers without breaking as they propagate towards the structure and exceed the structure freeboard, consequently inducing overtopping events. This can be clearly seen in the time series of WG11 to WG13. In WG11, the model is able to capture the overtopping events with a good match in phase. Even if the fluid layer on the top of the structure is very thin, the model is able to predict the measured free surface time series well in terms of phase and reasonably well when considering the amplitudes. An overestimation of wave height is visible in some waves of the record, resulting in an overprediction of some overtopping events as seen in WG11. One source of slight deviations could be the high reflection induced by the structure, almost 90%, which may increase the differences between the numerical absorption based on a sponge layer and the way active absorption in the flume deals with high reflection.

Similar results have been found for all the cases simulated but they have not been shown. Therefore, it can be concluded that the general agreement between experimental and numerical free surface time series is good for both regular and irregular waves.

5.2. Zero-order moment wave height

In order to provide a clearer insight into the behavior of the numerical model along the wave flume, a spectral analysis has been carried out. Zero-order moment wave height has been evaluated at different positions along the wave flume for both regular and irregular wave tests, with the purpose of analyzing the ability of the model to simulate wave energy evolution. The whole set of numerically simulated cases (14 for regular waves and 18 for irregular waves) has been compared with the experimental records. Fig. 3 shows the comparisons for the irregular wave tests. The presented panel displays results for the entire simulated and recorded set of cases at the gauges location in front of the caisson. The panel at the bottom right of Fig. 3 displays the zero-order moment wave heights at all the recorded locations and includes all the tested cases.

Results confirm that the model predicts very well the wave energy distribution along the flume. The accuracy is quite good, not only at the vicinity of the structure but also in the far field. The relative error for all tested cases has been calculated to be less than 5%, yielding -3.29% for regular and -0.61% for irregular waves. The standard deviation of the relative error has been found to be $\pm 8.04\%$ and $\pm 6.88\%$, for regular and irregular waves, respectively, showing a narrow deviation band of the results.

It should be noted that the error has been evaluated as the difference between the computed and the measured value, divided by the measured value.

5.3. Pressures

Pressure time series underneath and at the seaward face of the caisson are studied. Fig. 4 shows comparisons between predicted and experimental pressure time series: $H_s = 0.18$ m and $T_p = 5$ s. The upper panel in the plot presents the location of the 10 pressure gauges on the caisson. Comparisons show that the numerical model is able to represent with good accuracy the pressure time series except for minor deviations in magnitude present for some of the waves. The model seems to deal very well with the porous flow underneath the caisson, as can be seen in PG7 to PG10, as these records depend completely on the flow passing through the rubble-mound layers. It has to be pointed out that the porous flow parameters calibrated for two regular wave cases give outstanding results for irregular wave trains, too. Furthermore, numerical predictions of pressure at gauges PG5 and PG6, mostly registering only overtopping waves, are also very good. A correct evaluation of the pressure time series at the caisson is a fundamental issue to address structure stability considering the numerical model.

Fig. 5 shows simultaneous snapshots of free surface, velocities and pressure at four instants. The lower panel presents the comparison between the computed free surface time series and the experimental data. The left panel shows the comparison between the measured and calculated pressure law around the caisson at the selected times. The agreement is very good, both in the fluid and in the rubble-mound foundation. In the right panels, snapshots of free surface and velocity fields are plotted. The velocity field is presented at four instants in which the wave crest is reaching the structure. In the last panel at $t = 128.5$ s, the velocity field induced by an overtopped wave is presented. Note how the larger velocities are reached at the upper face of the caisson. Moreover, at $t = 122.8$ and 128.5, under overtopping conditions, the model is able to predict the pressure distribution both in front and underneath the caisson with very good accuracy. The results shown in this plot can be seen as an example of how the numerical model may contribute to complete physical model results by providing: (1) information of relevant variables with higher resolution; (2) time series in locations where measurements are difficult or not possible to take and (3) information of non-measured variables, such as in this particular case the velocity field.

6. Application of the model to wave overtopping analysis

An important potential application of the model is the evaluation of wave overtopping as one of the most relevant hydraulic parameters in the design of coastal structures. In this section, results obtained from the numerical model are compared with experimental results and existing wave overtopping formulae. Average overtopping discharge, percentage (probability) of

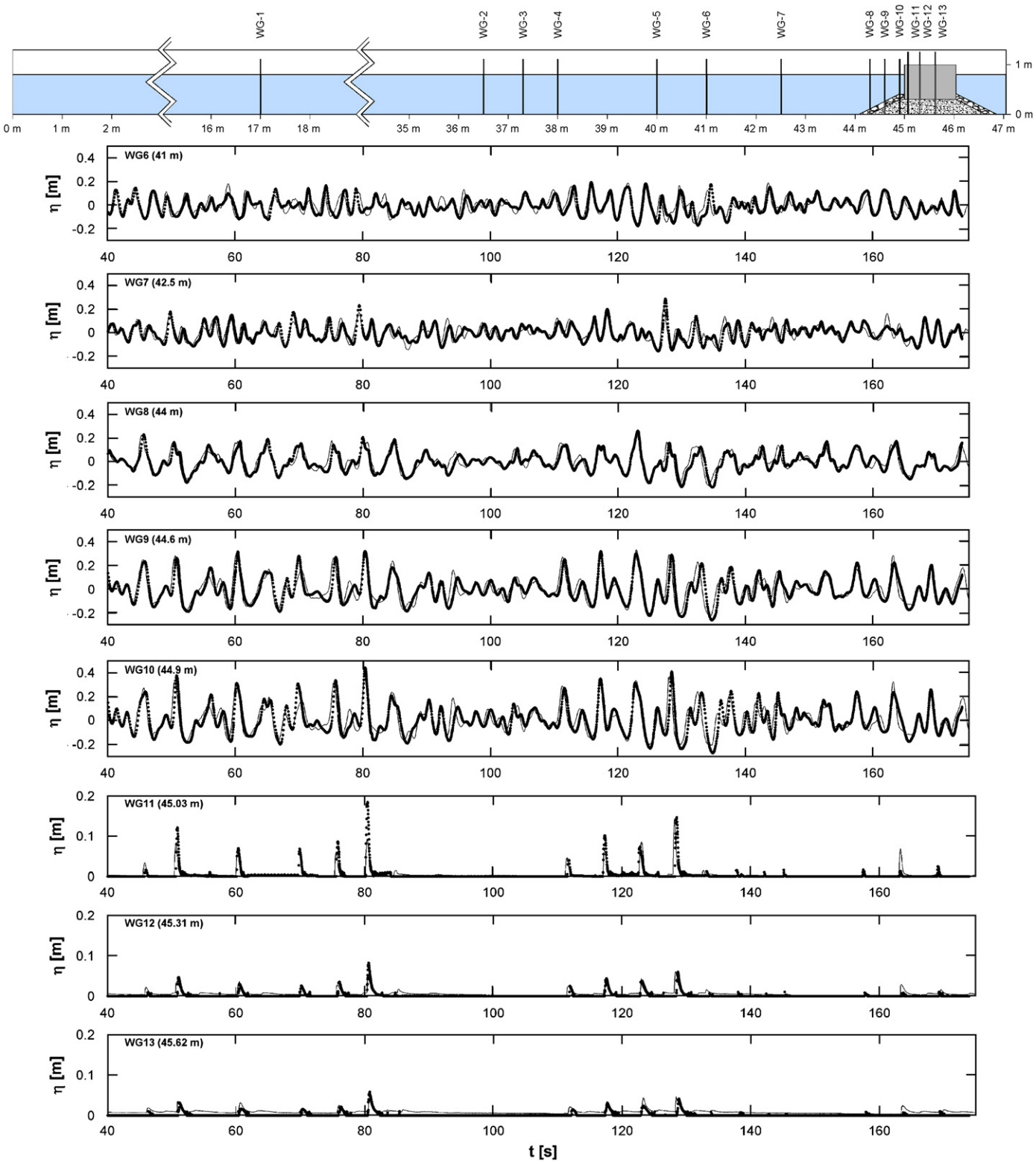

Fig. 2. Free surface evolution, solid line: laboratory measurements, dotted line: numerical results. Case ia55: $H_s = 0.18$ m, $T_p = 5$ s.

overtopping waves, maximum overtopping volume per wave and overtopping layer thickness are considered in order to validate the model capability to simulate wave overtopping.

One of the main advantages of using COBRAS-UC is that it is able to provide a time history of wave overtopping therefore opening the opportunity to analyze individual overtopping events which could be more important than the average discharge.

6.1. Analysis of average overtopping discharges

The accumulated overtopping discharge and the average discharge during the simulation period, Q_A, are shown in Fig. 6 for three irregular wave cases: $H_s = 0.21$ m and $T_p = 3$ s (left), $H_s = 0.18$ m and $T_p = 5$ s (middle) and $H_s = 0.18$ m and $T_p = 6$ s (right).

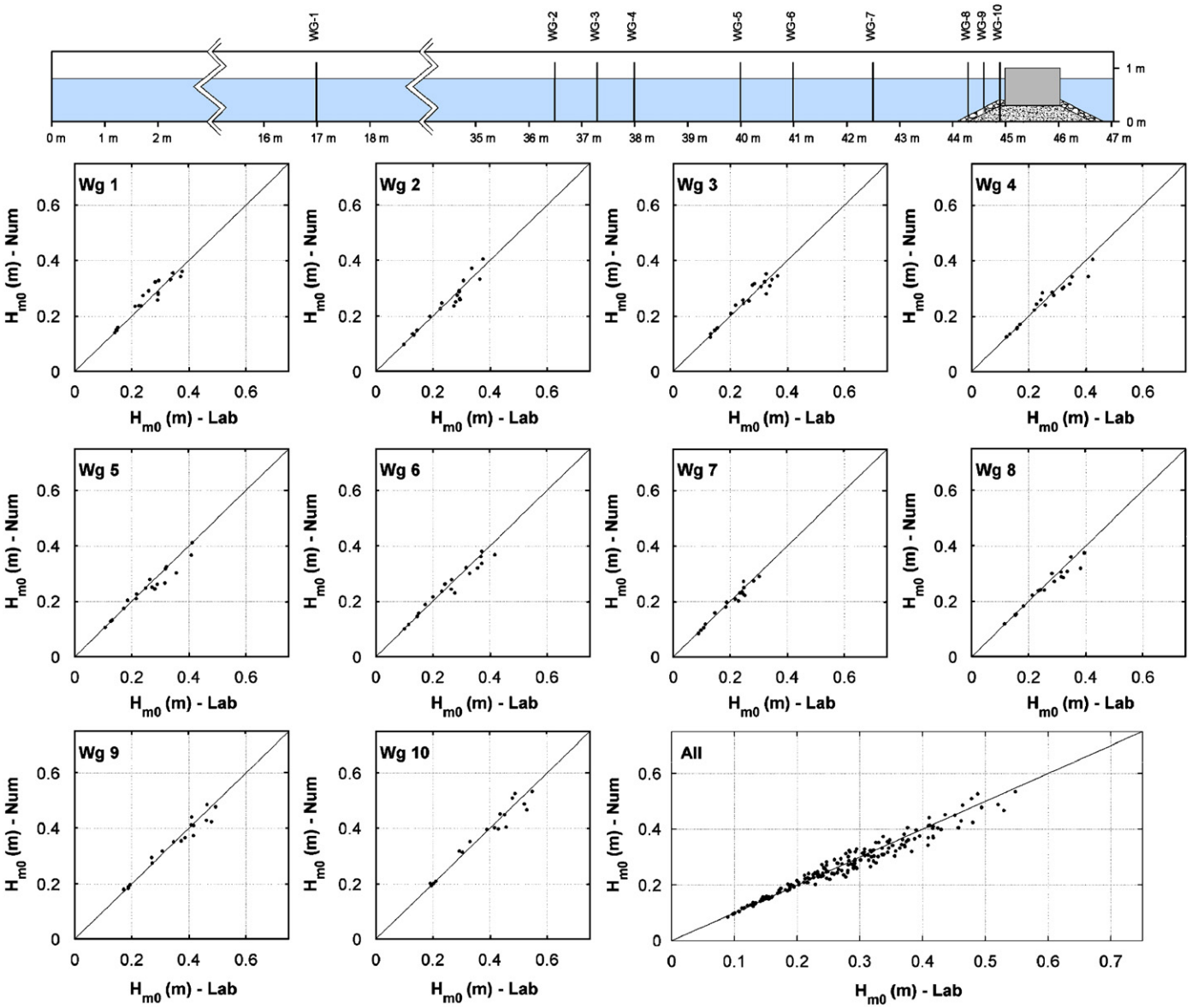

Fig. 3. Zero-moment wave height. Laboratory and numerical comparison—irregular wave cases.

In the three different cases, although minor differences exist, a good agreement between the numerical and the experimental accumulated overtopping discharge time history has been found. Only during short interval periods, some differences appear in the time series of wave overtopping volumes, due to the fact that slight differences in wave height deviations in front of the structure induce significant changes in the amount of water overtopped, as previously explained. The best agreement is found for the highest waves and shorter wave periods. Experimental and numerical results show that, since for the simulated cases the difference in wave height is small, overtopping is mostly controlled by the wave period.

The comparison between the numerical and the experimental average discharge over the simulation period shown in the plots, indicates relatively small differences, proving the abilities of COBRAS-UC to simulate, with a high degree of accuracy, the wave overtopping process in complicated structures.

Fig. 7 presents the average overtopping discharge values predicted by COBRAS-UC versus the experimental values for all the cases tested in the laboratory, including wave overtopping events. As can be seen, the model gives a good agreement showing a small general trend underestimating the experimental results, especially for small discharge values.

Fig. 7 also includes results obtained from semi-empirical formulae available in literature and applicable to the typology studied in this work. Franco et al. (1994) considered several configurations, including a vertical wall with and without a perforated front and a composite structure setup. The formulation by Besley (1999) is based on previous works by Bradbury and Allsop (1988) and Owen (1980) and considers low-mound breakwaters among other typologies.

Results show that the best agreement between numerical and experimental results is obtained by COBRAS-UC. The mean error of the numerical model is -8.5% with a standard deviation of $\pm 25.66\%$. Franco et al. (1994) show a worse agreement with a mean error of -71.9%, with a standard deviation of $\pm 25.66\%$. Besley (1999) formulation exhibits similar results to those shown by Franco et al. (1994), with a mean error of -63.4%, and a

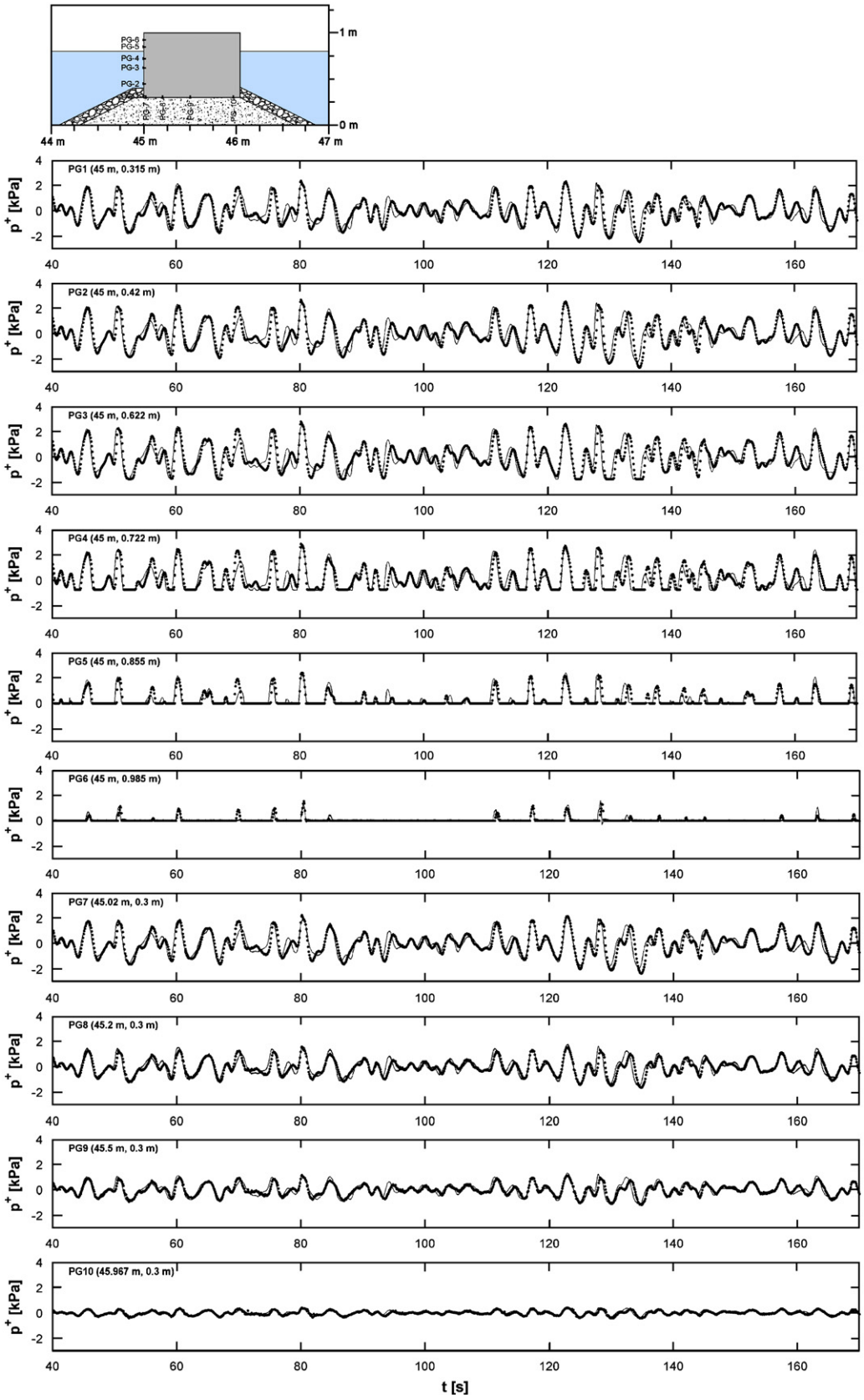

Fig. 4. Pressure time evolution, solid line: laboratory measurements, dotted line: numerical results. Case ia55: $H_s = 0.18$ m, $T_p = 5$ s.

standard deviation of $\pm 14.7\%$. In these typologies wave propagation is conditioned by the presence of the rubble mound, including the effect of pulsating waves. These results are not surprising since the formulae, probably the best ones available for this structure typology, were calibrated on different structural types, geometries and sets of experiments, while the numerical

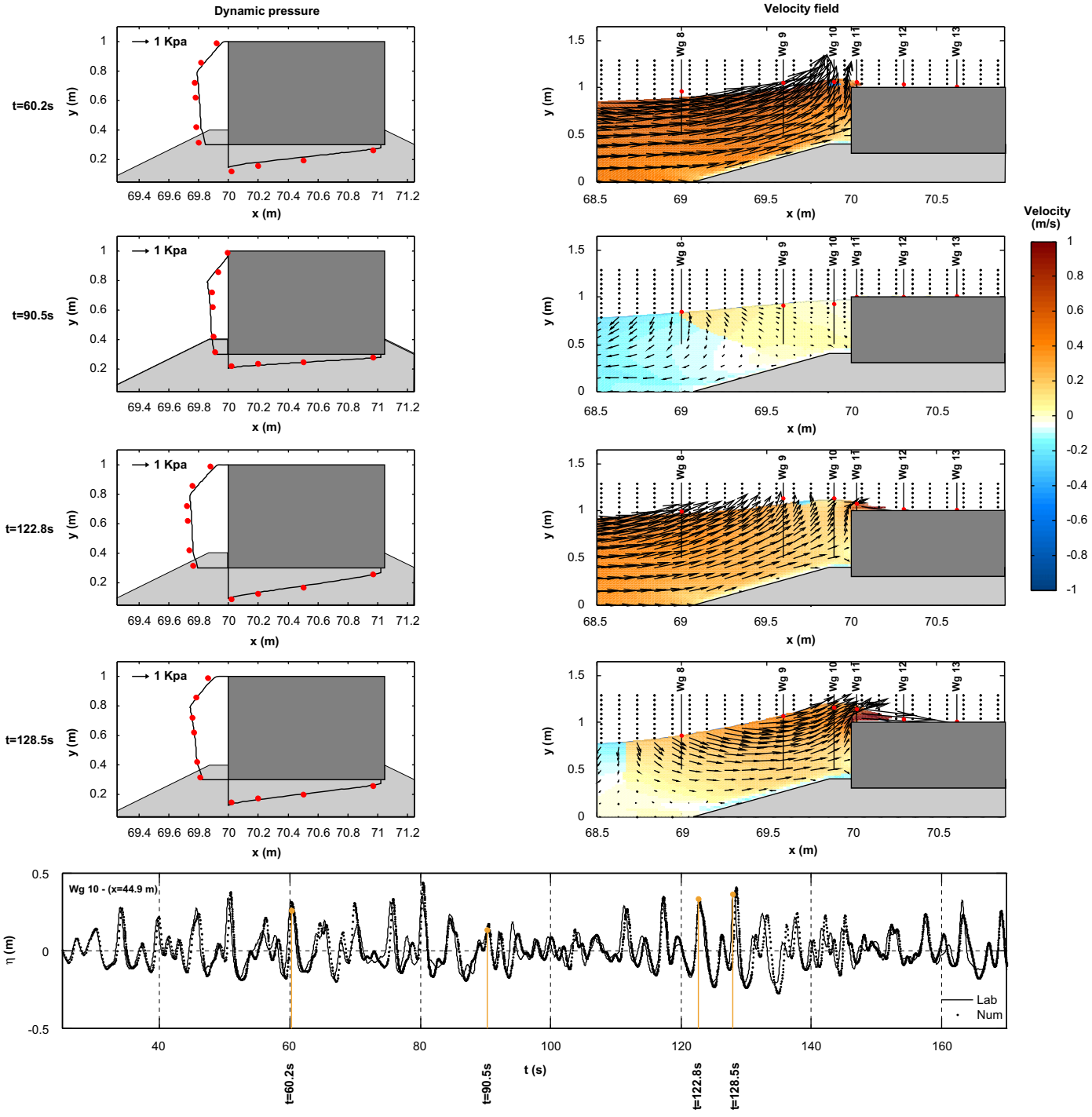

Fig. 5. Snapshots of instantaneous free surface, velocities and dynamic pressure.

modeling has been tailored specifically for these setups and the porous flow was calibrated for two tests.

6.2. *Percentage of overtopping waves and maximum overtopping event*

Overtopping events present a random distribution both in time and volume discharge and usually a small number of waves control the main part of the overtopped amount of water. According to Franco et al. (1994) and Franco and Franco (1999) the exceedance probability of each overtopping volume $P(V)$ can be calculated with a three-parameter Weibull distribution function, which is found to give a good statistical description of the data. This probability can be expressed in terms of three fitting coefficients A, B and C, which are the scale, shape and set-off fitting coefficients, respectively. The set-off coefficient C, represents the percentage (probability) of overtopping waves (N_{ow}/N_w), where N_{ow} and N_w are the number of overtopping waves and number of incident waves, respectively. Assuming the percentage of overtopping waves to be Rayleigh distributed, Franco et al. (1994) defines the following expression for C:

$$C = \frac{N_{ow}}{N_w} = \exp\left(-\left(\frac{1}{k}\frac{R_c}{H_s}\right)^2\right),$$

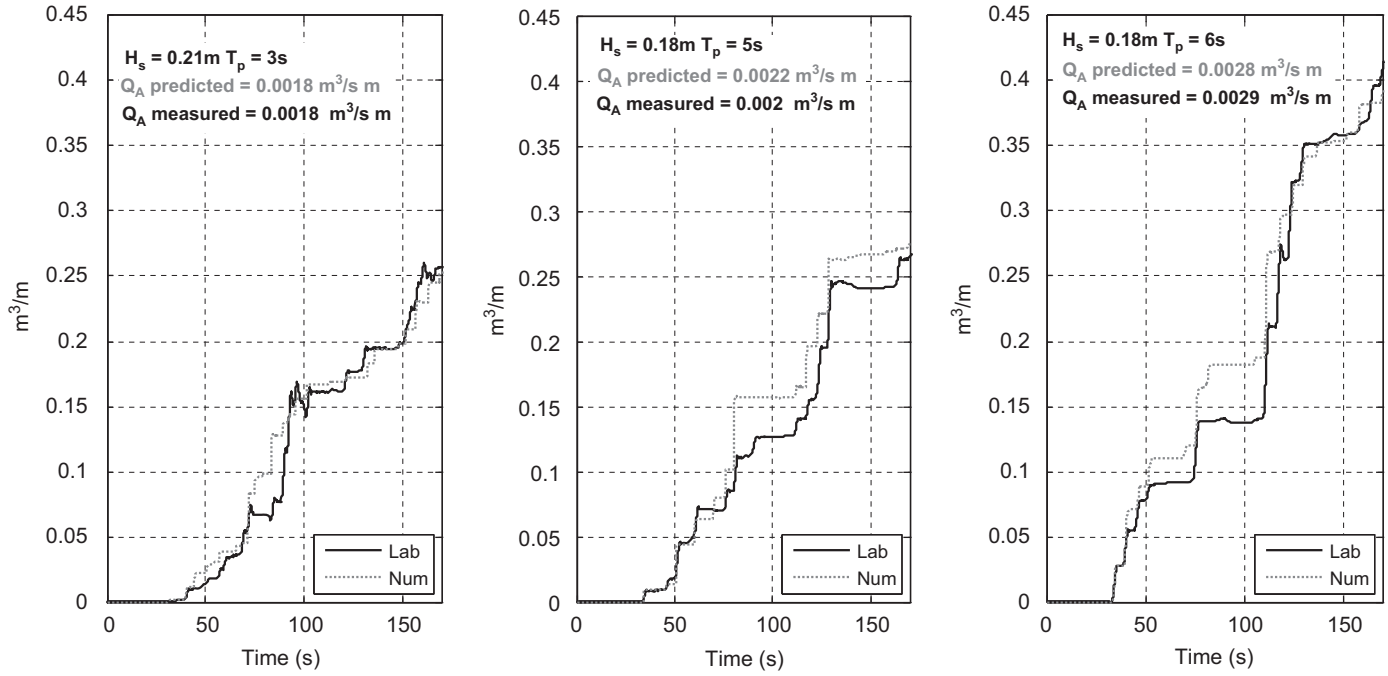

Fig. 6. Wave overtopping as a function of time.

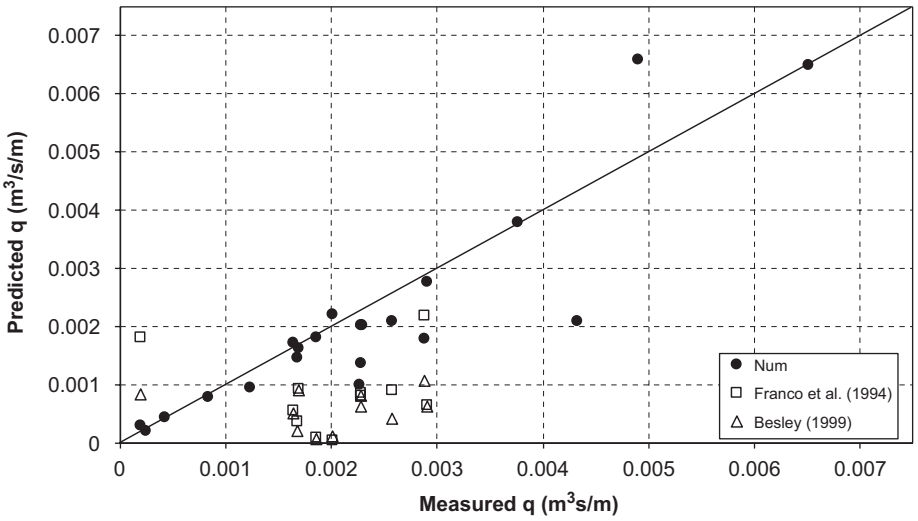

Fig. 7. Mean wave overtopping discharge—comparison between semi-empirical formulation, model and laboratory.

where k is a best fitting constant recommended to be 0.91 for caisson breakwaters.

Fig. 8b presents the comparison between probability of overtopping, represented by the set-off coefficient, C, observed in the laboratory versus the values predicted by the model and the formulation by Franco et al. (1994). The numerical results show a good agreement with the measurements as expected because the average overtopping discharges were correctly simulated. Cases with an overtopping probability of 1 or close to 1, correspond to highly energetic regular waves. Cases with a probability of 0 or close to 0, correspond to irregular and regular wave cases with low wave heights, and consequently, with no overtopping events.

The maximum overtopping event is an alternative parameter in the analysis of hydraulic response since, in general, a few overtopping events may dominate the functionality performance of a coastal structure. Maximum overtopping event comparison is plotted on Fig. 8a showing a relatively good agreement with a general trend to underestimate the experimental values. COBRAS-UC shows a mean error of -13.5% with a standard deviation of $\pm 32\%$.

6.3. Overtopping layer thickness

COBRAS-UC provides the possibility to analyze the behavior of the flow on the top of the caisson once the wave has overtopped the structure. In this case, the overtopped water layer thickness deformation is considered.

In Fig. 9, the comparison between the mean water layer thickness determined numerically and the value computed from the three gauges located at the top of the caisson (Wg 11, Wg 12 and Wg 13) is plotted. As can be seen, the agreement between the

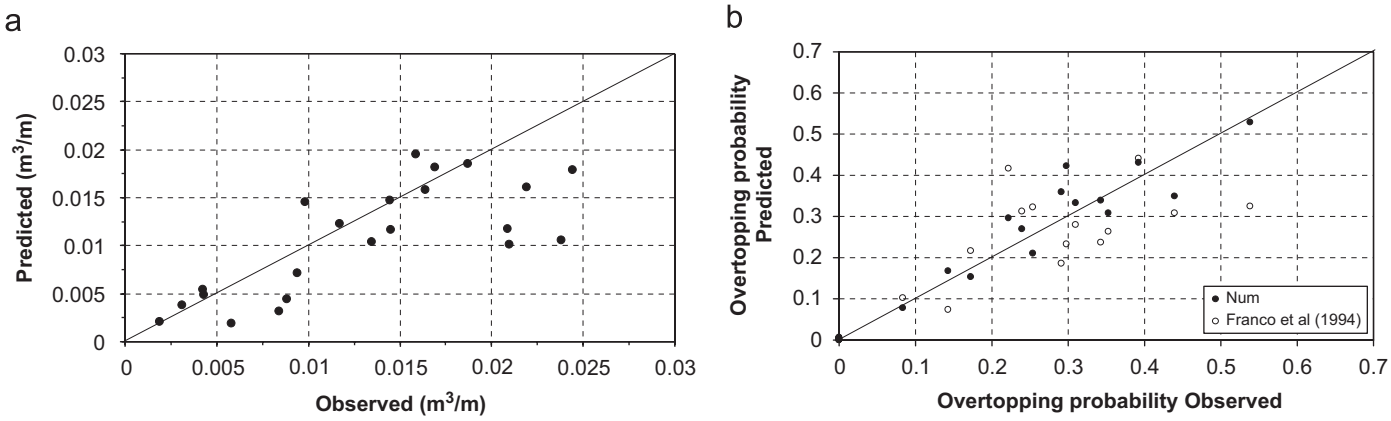

Fig. 8. (a) Comparison between experimental, numerical and semi-empirical results for maximum overtopping volume. (b) V_{max} set-off coefficient $C=(N_{ow}/N_w)$ representing the percentage of overtopping wave. Comparison between numerical, semi-empirical and observed values.

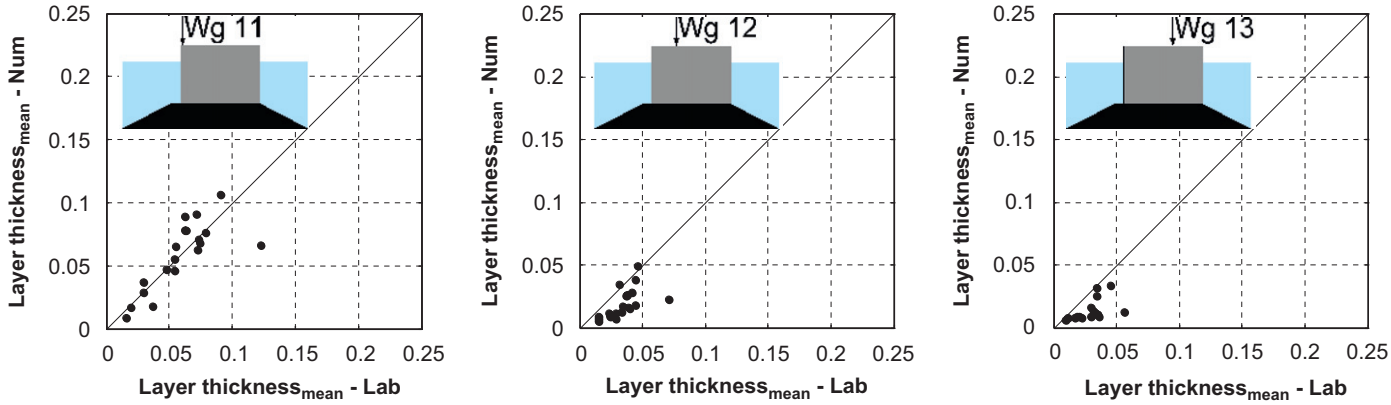

Fig. 9. Mean overtopping layer thickness at the caisson crest.

numerical and experimental values varies as the water flows towards the end of the caisson. The best agreement is found at the first location (Wg 11) where the mean error and standard deviation are -1.35% and $\pm 26.6\%$, respectively. However, at Wg 12 and Wg 13 the accuracy of the numerical model decreases resulting in an underprediction of the layer thickness. The main reason for these discrepancies lies on the fact that the thickness of the layer is drastically reduced, tending to become of the same order of magnitude as the cell size. The numerical setup considered does not have enough resolution to resolve the flow.

7. Comparison between low-mound and rubble-mound breakwaters

In this paper, wave interaction with a low-mound breakwater has been modeled using physical and numerical simulations. In Losada et al. (2008), a rubble-mound breakwater was studied using very similar experimental and numerical setups. Given the fact that the incident wave conditions and the structure freeboards considered are identical, a unique opportunity to compare the response of two different structure typologies is given.

As shown, the hydraulic response of low-mound breakwaters is dominated by reflection. Therefore, in order to reproduce the number of overtopping events and the volume discharge per event, the most accurate possible simulation of the free surface time series at the toe of the structure is required. Results have shown that this accuracy can only be achieved if re-reflected waves in the numerical wave flume are well absorbed. Porous flow modeling plays a relatively important role, but turbulence is almost negligible, at least at laboratory scale. Regarding rubble-mound breakwaters, wave absorption is of relative relevance since reflection is much lower. The most important processes requiring an accurate simulation are wave breaking and run-up on the structure. A correct modeling of turbulence and porous flow are extremely relevant to achieve this requirement.

Fig. 10 presents a comparison between maximum overtopping volumes obtained from physical modeling for both structures. The plot shows that the rubble-mound breakwater presents higher maximum overtopping volumes for almost all the different incident wave conditions considered. In several cases the maximum overtopping volumes in rubble-mound breakwaters are 20–30 times larger than for the low-mound breakwater.

Franco et al. (1994) and COBRAS-UC give a much better prediction of the overtopping probability for low-mound breakwaters than for rubble-mound breakwaters. For the same incident conditions, the percentage of overtopping waves is higher for rubble-mound breakwaters.

The mean wave overtopping discharge prediction based on the numerical model is similar for both typologies with small mean errors and a slightly higher standard deviation for the rubble-mound structure. Considering the previously mentioned limitation in the application of the empirical formulae to these cases, Franco et al. (1994) does work much better for rubble-mound breakwaters than for low-mound breakwaters. However, Besley (1999) is slightly better suited for low-mound breakwaters. For identical incident wave conditions and freeboard, the mean overtopping rate is almost 50% larger for rubble-mound

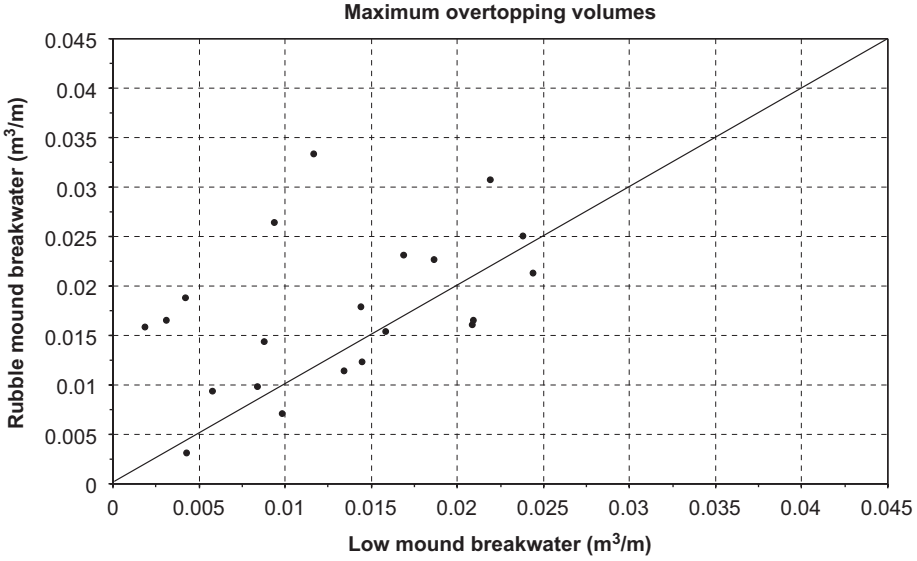

Fig. 10. Comparison between maximum overtopping volumes obtained from physical modeling for rubble-mound (Losada et al., 2008) and low-mound breakwaters.

breakwaters. This factor may vary depending on rubble-mound characteristics, since decreasing porosity may increase run-up and consequently wave overtopping.

8. Recommendations for numerical modeling

After the integration of the analysis carried out in Losada et al. (2008) for rubble-mound breakwaters and for low-mound breakwaters in this work, several numerical and physical factors have to be taken into account when numerical analysis of wave overtopping using a RANS model is considered.

Based on our experience, the numerical resolution appears as a very important parameter. In order to define the vertical dimension of the water layer overtopping the structure, at least 5–10 cells have to be considered. Lower resolutions increase the uncertainty on the wave discharge calculations.

Wave generation procedure also appears to be very important to ensure target wave conditions close to the structure. The generation procedure has to take into account the waves reflected on the structure which reach the generation zone. This issue is extremely important in the study of highly reflective structures such as the present case. Several options on the generation procedure can be considered. The internal wave maker, first presented by Lin and Liu (1999) and later improved by Lara et al. (2006a, b), can only be applied to shallow water conditions and requires larger domains to include a numerical sponge to absorb reflective waves. Recently, Torres-Freyermuth (2007) presented a boundary condition which successfully absorbs the reflective waves, making the use of a sponge layer unnecessary, and therefore reducing the computational cost and the size of the domains. Future applications should be based on this generation procedure.

Among the physical factors which play an important role on the wave overtopping analysis, especially relevant are the turbulence and the porous media flow modeling.

Turbulence modeling in two-dimensional numerical flumes has been solved by mainly using a k–ε approximation, considering the empirical coefficients proposed by Rodi (1980). COBRAS-UC has been extensively validated on the wave breaking induced turbulence in laboratory scale, as presented in Lin and Liu (1998) on impermeable beaches and Lara et al. (2006a, b) on permeable beaches, and also in natural beaches, Torres-Freyermuth et al. (2007), demonstrating a good performance of the modeling approach. In all the referenced studies, the turbulence closer model coefficients were kept constant and were not used for the purpose of calibrating the model. One important issue is pointed out in Lara et al. (2006a, b) regarding the importance of the breaking wave-induced turbulence on porous layers. Lara et al. (2006a, b) demonstrated that the porous media generated turbulence has less importance on the momentum damping processes than the wave breaking. That is a crucial issue in the wave overtopping calculation of rubble-mound breakwaters, in which both breaking and porous media flow are present, since it implies that models including porous flow modeling but failing in the modeling of the wave breaking process and associated turbulence, will give inaccurate run-up and overtopping results. One way to mitigate this problem is by smoothing out the inaccuracies in the breaking modeling by tuning the porous media model parameters to adjust dissipation. However, there is no physical meaning in this approach and it should be avoided.

Regarding porous media flow, both aspects have to be considered. Based on our experience, the most important parameter in the wave overtopping is the porosity of the porous media. Variations of only 10% of this parameter can produce overtopping events in a non-expected overtopped structure.

The scale effects, which are also present on the empirical formulations used nowadays for design, are also an important factor to keep in mind. This issue is still today an ongoing task in the literature because the limited existing information on prototype scale to evaluate the uncertainty assumed for the formulations. The numerical model reveals itself as an important tool to be used in the study of wave overtopping or on other functional magnitudes.

9. Conclusions

In this paper, the application of a model, named COBRAS-UC to the analysis of wave interaction with low-mound breakwaters is presented. The equations considered in the model allow the simulation of complex 2-D flows including transient, highly nonlinear waves, wave breaking and porous flow. The model allows long simulations that can vary from hundreds to thousands

of waves depending on resolution, in reasonable periods of time and on standard PCs. The numerical model has been validated against a set of experimental cases including regular and irregular waves. Results have shown that the model is capable of predicting the hydraulic response of the structure very well.

Furthermore, the analysis of wave overtopping has also shown that COBRAS-UC has a high potential to become a complementary tool to analyze the hydraulic response of this typology of structures. It has been shown that the model may contribute to improve physical modeling by providing: (1) information of relevant variables with higher resolution; (2) time series in locations where measurements are difficult or not possible to take and (3) information of non-measured variables.

In order to improve the model capacities and especially to provide important statistical information for the analysis of structure response, the computational efficiency of the model still requires improvement, since for certain grid resolutions, simulations including about 1000 waves may require several days of computation on a standard PC. Moreover, further work has to be carried out in order to validate the model at prototype scale.

Regarding new processes, the introduction of air or 3-D effects might be of importance under some circumstances in the modeling.

Acknowledgments

The authors are indebted to Puertos del Estado (State Ports of Spain) for the partial funding provided to carry out this research. J.L. Lara is indebted to the M.E.C. for the funding provided in the Ramon y Cajal Program.

References

Besley, P., 1999. Overtopping of seawalls: design and assessment manual. R&D Technical Report No. W178, Environment Agency, Bristol, 37pp., CEM, Coastal Engineering Manual.

Bradbury, A.P., Allsop, N.W.H., 1988. Hydraulic effects of breakwaters crown walls. In: Proceedings of the Conference on Design of Breakwaters. Institution of Civil Engineering, Thomas Telford, London, pp. 385–396.

Burcharth, H.F., Hughes, S.A., 2006. Fundamentals of design—Part 1, Chapter 1, 2 and 3. In: Vincent, L., Demirbilek, Z. (Eds.), Coastal Engineering Manual, Part II, Hydrodynamics, Chapter II-2, Engineer Manual 1110-2-1100. US Army Corps of Engineers, Washington, DC.

Dalrymple, R.A., Knio, O., Cox, D.T., Gomez-Gesteira, M., Zou, S., 2001. Using a Lagrangian particle method for deck overtopping. In: Proceedings of the Waves ASCE 2001, pp. 1082–1091.

Franco, C., Franco, L., 1999. Overtopping formulas for caisson breakwaters with nonbreaking 3D waves. Journal of Waterway, Port, Coastal, and Ocean Engineering, American Society of Civil Engineers 125 (2), 98–108.

Franco, L., de Gerloni, M., van der Meer, J.W., 1994. Wave overtopping on vertical and composite breakwaters. In: Proceedings of the 24th International Coastal Engineering Conference, American Society of Civil Engineers, vol. 1, pp. 1030–1045.

Garcia, N., Lara, J.L., Losada, I.J., 2004. 2-D Numerical analysis of near-field flow at low-crested permeable breakwaters. Coastal Engineering 51, 991–1020.

Gotoh, H., Shao, S.D., Memita, T., 2004. SPH–LES model for numerical investigation of wave interaction with partially immersed breakwater. Coastal Engineering of Japan 46 (1), 39–63.

Hsu, T.-J., Sakakiyama, T., Liu, P.L.-F., 2002. A numerical model for wave motions and turbulence flows in front of a composite breakwater. Coastal Engineering 46, 25–50.

Hu, K., Mingham, C.G., Causon, D.M., 2000. Numerical simulation of wave overtopping of coastal structures using the non-linear shallow water equations. Coastal Engineering 41, 433–465.

Hubbard, M.E., Dodd, N., 2002. A 2D numerical model of wave run-up and overtopping. Coastal Engineering 47, 1–26.

Kawasaki, K., 1999. Numerical simulation of breaking and post-breaking wave deformation process around a submerged breakwater. Coastal Engineering Journal 41, 201–223.

Kobayashi, N., Wurjanto, A., 1989. Wave transmission over submerged breakwaters. Journal of Waterways, Port, Coastal and Ocean Engineering 115, 662–680.

Koshizuka, S., Tamako, H., Oka, Y., 1995. A particle method for incompressible viscous flow with fluid fragmentation. Computational Fluid Dynamics Journal 4 (1), 29–46.

Kothe, D.B., Mjolsness, R.C., Torrey, M.D., 1991. RIPPLE: a computer program for incompressible flows with free surfaces. Los Alamos National Laboratory, LA-12007-S.

Lara, J.L., Garcia, N., Losada, I.J., 2006a. RANS modelling applied to random wave interaction with submerged permeable structures. Coastal Engineering 53, 395–417.

Lara, J.L., Losada, I.J., Liu, P.L.-F., 2006b. Breaking waves over a mild gravel slope: experimental and numerical analysis. Journal of Geophysical Research, AGU 111, C11019.

Li, T., Troch, P., De Rouck, J., 2004. Wave overtopping over a sea dike. Journal of Computational Physics 198, 686–726.

Lin, P.Z., Liu, P.L.F., 1998. A numerical study of breaking waves in the surf zone. Journal of Fluid Mechanics 359, 239–264.

Lin, P., Liu, P.L.-F., 1999. Internal wave-maker for Navier-Stokes equations models. Journal of Waterway, Port, Coastal, and Ocean Engineering (ASCE) 125 (4), 207–215.

Losada, I.J., 2003. Advances in modeling the effects of permeable and reflective structures on waves and nearshore flows. In: Chris Lakhan, V. (Ed.), Advances in Coastal Modeling. Elsevier Oceanography Series, vol. 67.

Losada, I.J., Lara, J.L., Damgaard, E., Garcia, N., 2005. Modelling of velocity and turbulence fields around and within low-crested rubble-mound breakwaters. Coastal Engineering 52, 887–913.

Losada, I.J., Lara, J.L., Guanche, R., Gonzalez-Ondina, J.M., 2008. Numerical analysis of wave overtopping of rubble mound breakwaters. Coastal Engineering 55.

Lynett, P., Liu, P.L.-F., Losada, I.J., Vidal, C., 2000. Solitary wave interaction with porous breakwaters. Journal of Waterway, Port, Coastal, and Ocean Engineering (ASCE) 126 (6), 314–322.

Mingham, C.G., Causon, D.M., 1998. High-resolution finite-volume method for shallow water flows. Journal of Hydraulic Engineering, ASCE 124 (6), 605–614.

Oumeraci, H., et al., 2001. Probabilistic Design Tools for Vertical Breakwaters. A.A. Balkema Publishers, 373pp.

Owen, M.W., 1980. Design of sea walls allowing for wave overtopping. Report EX 924, Hydraulics Research, Wallingford.

Rodi, W., 1980. Turbulence Models and their Application in Hydraulics—a State-of-The-Art Review. IAHR Publication.

Shao, S., 2006. Incompressible SPH simulation of wave breaking and overtopping with turbulence modeling. International Journal of Numerical Methods and Fluids 50, 597–621.

Stansby, P.K., Feng, T., 2004. Surf zone wave overtopping a trapezoidal structure: 1-D modelling and PIV comparison. Coastal Engineering 51, 483–500.

Torres-Freyermuth, A., 2007. Numerical analysis of surf zone hydrodynamics based on RANS equations. Ph.D. Thesis. Universidad de Cantabria.

Torres-Freyermuth, A., Losada, I.J., Lara, J.L., 2007. Modeling of surf zone processes on a natural beach using Reynolds-Averaged Navier–Stokes equations. Journal of Geophysical Research 112, C09014.

Troch, P., de Rouck, J., 1998. Development of two-dimensional numerical wave flume for wave interaction with rubble mound breakwaters. In: 26th International Coastal Engineering Conference, pp. 1638–1649.